

1 **NO₂ seasonal evolution in the North Subtropical free** 2 **troposphere**

3

4 **M. Gil-Ojeda¹, M. Navarro-Comas¹, L. Gómez-Martín¹, J.A. Adame¹, A. Saiz-**
5 **Lopez², C. A. Cuevas², Y. González³, O. Puentedura¹, E. Cuevas³, J-F**
6 **Lamarque⁴, D. Kinninson⁴ and S. Tilmes⁴**

7 [1]{Instituto Nacional de Técnica Aeroespacial, Torrejón de Ardoz, Spain }

8 [2]{Atmospheric Chemistry and Climate Group, Institute of Physical Chemistry Rocasolano,
9 CSIC, Madrid, Spain }

10 [3]{Izaña Atmospheric Research Center, AEMET, Tenerife, Spain }

11 [4]{Atmospheric Chemistry Division, NCAR, Boulder, CO, USA }

12 Correspondence to: M. Gil-Ojeda (gilm@inta.es)

13

14 **Abstract**

15 Three years of Multi-Axis Differential Optical Absorption Spectroscopy (MAXDOAS)
16 measurements (2011-2013) have been used for estimating the NO₂ mixing ratio along a
17 horizontal line of sight from the high mountain Subtropical observatory of Izaña, at 2370 m
18 a.s.l. (NDACC station, 28.3°N, 16.5°W). The method is based on horizontal path calculation
19 from the O₂-O₂ collisional complex at the 477 nm absorption band which is measured
20 simultaneously to the NO₂, and is applicable under low aerosols loading conditions.

21 The MAXDOAS technique, applied in horizontal mode in the free troposphere, minimizes the
22 impact of the NO₂ contamination resulting from the arrival of MBL airmasses from thermally
23 forced upwelling breeze during central hours of the day. Comparisons with in situ
24 observations show that during most of measuring period the MAXDOAS is insensitive or
25 very little sensitive to the upwelling breeze. Exceptions are found under pollution events
26 during southern wind conditions. On these occasions, evidence of fast efficient and
27 irreversible transport from the surface to the free troposphere is found.

28 Background NO₂ vmr, representative of the remote free troposphere, are in the range of 20-45

1 pptv. The observed seasonal evolution shows an annual wave where the peak is in phase with
2 the solar radiation. Model simulations with the chemistry-climate CAM-Chem model are in
3 good agreement with the NO₂ measurements, and are used to further investigate the possible
4 drivers of the NO₂ seasonality observed at Izaña.

5

6 **1 Introduction**

7 Nitrogen oxides play an important role in tropospheric chemistry as they control the O₃
8 photochemical catalytic production (Crutzen, 1979), the abundance of hydroxyl radicals, and
9 contribute to the nitrate aerosols formation. In a background unpolluted atmosphere where
10 NO_x concentrations are low, net ozone loss occurs during photochemically active periods (Liu
11 et al., 1983; Isaksen et al., 2005). NO_x abundance is highly variable since it is influenced by
12 non-steady natural and anthropogenic emissions and its global distribution is still uncertain.
13 Free Troposphere (FT) source inventories indicate that major production comes from lightning
14 (2-16 Tg N yr⁻¹), followed by NH₃ oxidation (0.3-3 Tg N yr⁻¹), stratospheric intrusion (0.08-1
15 Tg N yr⁻¹) and aircraft (0.6-0.7 Tg N yr⁻¹). Contribution from the boundary layer in remote
16 regions is rare (Bradshaw et al., 2000).

17 Information of surface NO_x on polluted areas is available due to extended governmental air
18 quality networks. During the last decade, satellite instruments have demonstrated capabilities
19 for successful retrieval of tropospheric NO₂ identifying enhanced concentrations over urban
20 and industrial areas in the boundary layer (Richter et al., 2005; Irie et al., 2005) and tracking
21 the temporal trends (Hilboll et al., 2013; Cuevas et al., 2014). However, direct NO₂
22 measurements in the background FT are scarce due to the requirement of observational
23 platforms above, typically 2000 m a.s.l., but also due to the low concentrations present at
24 those levels.

25 Airborne NO₂ measurements have been performed for decades (Ridley et al., 1988; Carroll et
26 al., 1990), however the need for very short response times at concentrations close to the
27 instrumental detection limit, make the FT observations a challenging task. Even though well
28 characterized aircraft instruments reach detection limits as low as 10 pptv (Heland et al.,
29 2002), few studies are reported in the literature. Measurements are generally collected during
30 individual field campaigns associated to specific targets such as chemistry missions or
31 satellite validations (Jacob et al., 2003; Bucsela et al., 2008; Boersma et al., 2008; Baidar et

1 al., 2013; Flynn et al., 2014). These time and space sparse data limit the study of seasonalities
2 or trends in the FT. Only recently, attempts to obtain global FT NO₂ abundances from satellite
3 OMI instrument has been performed for the first time (Choi et al., 2014) by using the cloud
4 slicing technique (Ziemke 2001). The method is based on the comparison of cloud and
5 cloudless scenes to derive the FT mean concentrations. Results show that valuable
6 information on NO₂ large scale phenomena can be derived on areas where clouds presence is
7 frequent but does not provide results in places such as East Atlantic subtropical latitudes
8 where high pressures are dominant features.

9 Instruments operating in the few high mountain stations existent around the world are the only
10 alternative to monitor NO₂ in the background FT. However, the in situ measurements are
11 often affected by the “upslope breeze effect” (Kleissl et al., 2007; Val Martin et al., 2008;
12 Rodriguez et al., 2009; Reidmiller et al., 2010; Cuevas et al., 2013). Radiative heating in the
13 mountain slopes result in air upwelling from the boundary layer contaminating the daytime
14 measurements by generally larger values over the polluted lower layers.

15 Recently, Gomez et al. (2014) have presented a simple method based on a Modified
16 Geometrical Approximation (MGA) to estimate trace gases concentrations at the level of the
17 Izaña Observatory from MAXDOAS measurements. The horizontal path length is obtained
18 from the oxygen collisional complex (O₄, hereafter) simultaneously measured with the tracer
19 under consideration (NO₂ and O₃). Gomez et al. examined a short summer period to
20 demonstrate the validity of the method. Here we apply the same technique to data covering 3
21 full years (2011-2013) to analyze the seasonal evolution of the NO₂ concentrations in volume
22 mixing ratio (vmr). MAXDOAS present two main advantages with respect to the in situ
23 instrument at this location, both related to the very long optical path of the measurements of
24 over 60 km. Firstly, it minimizes the potential contribution of NO₂ that may be upwelled from
25 the marine boundary layer (MBL). The breeze layer has a limited vertical extension and its
26 relative contribution to the MAXDOAS long path is small. On the contrary, Izaña in situ data
27 around noon are strongly influenced by the underlying polluted MBL (Puentedura et al.,
28 2012; Gomez et al., 2014). Secondly, due to the long light paths achieved by MAXDOAS in
29 the FT, very low concentrations, of few ppt, can be measured.

30 Section 2 presents the method, limits and associated errors. In Sect. 3 the station and data sets
31 are depicted. Section 4 describes the method used for profiles retrieval. The description of the
32 chemical and back trajectories models is done in Sect. 5. Finally, Sects. 6 and 7 present the

1 results and discussion, and summary, respectively.

2

3 **2 Instrument and methodology**

4 In year 2010 the DOAS spectrometer, operating in zenith mode at that time, was upgraded for
5 MAXDOAS measurements. The spectrometer records the sky spectrum in the visible range at
6 a spectral resolution of 0.55 nm in 10 elevation angles from -1 to 90°, and 1° field of view
7 covering a full cycle in 20 min. The number of cycles per day ranges from 26 at winter
8 solstice to 38 in summer. NO₂ is evaluated in the 425-520 nm range in order to
9 simultaneously retrieve the O₄ from the 477 nm absorbing band. The scanning plane is on 0°
10 azimuth (North) to minimize the dependence of the path with the azimuth (Wittrock et al.,
11 2004). The instrument is part of the Network for the Detection of the Atmospheric
12 Composition Change (NDACC) and other settings are those recommended for DOAS type
13 spectrometers. NO₂ at 294K temperature from Vandaele et al. (1998) and O₄ from Hermans et
14 al. (1990) cross sections have been used. Details of the instrument, settings and operational
15 mode can be found in Puentedura et al. (2012) and Gomez et at. (2014).

16 The Modified Geometry Approximation (MGA) described in Gomez et at., (2014) has been
17 used for the data analysis. NO₂ vmr at the level of the station is obtained by dividing the
18 differential slant column density (DSCD) measured in the horizontal geometry by the
19 horizontal optical path. The DSCD is obtained by subtracting the measurement obtained at the
20 zenith (SZA=90°) from the measurement in the horizontal path. In a first approximation, the
21 slant paths contributions of 0 and 90° geometries cancel out and only the signal of the tracers
22 present in the horizontal path remains (See Gomez et al., 2014 for details). The method
23 assumes a quasi-Rayleigh atmosphere, i.e. very low Aerosol Optical Depth (AOD), and a
24 single scattering before the photon reaches the detector. The path is obtained from the O₄
25 horizontal column since the amount of O₂ is known from the independent air pressure
26 measurements. The path length is then corrected to account for the differences in wavelengths
27 between the O₄ and NO₂ analysis ranges. In practice, the scattering of the zenith path does not
28 take place near the instrument but at a few km above the level of the station. The actual
29 concentration of a measured species X at the station level is given by:

30

$$31 \quad X_{vm} = \frac{X_{DSD}}{\frac{Q_{DSD}}{Q_{ref}} f + \epsilon} \quad [1]$$

1
2
3
4
5
6
7
8
9
10

Where X_{DSCD} and O_{4DSCD} are the slant measured columns of the species X and O_4 , respectively. $[O_4]_{surface}$ is the O_4 at the level of the station, f is the correction factor due to differences in wavelength absorption ranges of the specie under study with respect to O_4 that can be computed from a radiative transfer model (RTM) and c is the error of the approach. The latter is a factor accounting for the dependence with the different vertical distributions of both species and AMFs.

$$c = h(Rg - R'g) \tag{2}$$

12

h is the effective scattering height of the vertical ray. R and R' are the ratio of the mean concentration of the layer divided by the concentration at the level of the station of tracer X and O_4 , respectively, and g and g' accounts for their AMF in the zenith geometry ($g = AMF(SZA) - 1$), where SZA stands for Solar Zenith Angle.

The effective scattering height is defined as

$$h = \frac{\int_{surface}^{top} I(z) dz}{\int_{surface}^{top} I(z) dz} \tag{3}$$

21

where
$$\frac{I(z)}{\int_{surface}^{top} I(z) dz}$$

24 represents the normalized contribution of the ray scattered at each atmospheric layer to the total flux at surface. From radiative transfer calculations it can be shown that the effective scattering height ranges between 6.5 and 7.5 km above the station for solar zenith angle (SZA) below 70°, which we estimate as the validity limit of the method.

28 Since both NO_2 and O_4 are analyzed in the same spectral range, the difference between the

1 weighted center of the range for NO₂, i.e. the effective wavelength, and that of O₄ is small.
2 The value of f is of 0.9 for a near-Rayleigh atmosphere.

3 By using Eq. (2), the error introduced in NO₂ vmr due to the geometrical approximation, if
4 assuming a constant mixing ratio of both O₄ and NO₂ with height, is of 9.0 % at 70° SZA and
5 of 2.3% at 50°. Since the scattering heights and the air mass factors are well known, the data
6 can be corrected. The only uncertainty is due to the R value related to the vertical distribution
7 of NO₂ within the FT. However, aircraft measurements over the ocean far from large
8 industrial areas show that the tropospheric vertical distribution is nearly constant above the
9 MBL (Bucsela et al., 2008)

10 In the presence of moderate or high aerosols loading at the level of the observational point,
11 multiple scattering takes place and the method is no longer valid. Assuming that the aerosol
12 layer is a well mixed layer, we estimate the AOD=0.1 at 500 nm as a safe limit (Gomez et al.,
13 2014).

14 Since the path length is obtained from O₄ measurements, uncertainty in the magnitude of its
15 absolute cross section is an additional source of error. It has been reported that paths obtained
16 from O₄ are even larger than that RT computed for a Rayleigh atmosphere (Wagner et al.,
17 2002) when using the generally accepted cross-sections reported in literature (Greenblatt,
18 1990; Hermans et al., 1999), suggesting that cross-section are underestimated. There is,
19 however, no agreement in the magnitude of the correct values. We performed direct Sun
20 measurements on a very clear morning (Aerosol Optical Density at 500 nm over the
21 observatory = 0.007 ± 0.00077) at an O₄ effective temperature of 250 K, and compared the
22 retrieved slants columns with the ones calculated from the local radiosounding of the day (7
23 October, 2014) up to 30 km and the tropical standard atmosphere from 30 km upwards.
24 Results show an excellent agreement with no difference at the error level when the retrieval
25 includes O₄ cross-sections at two temperatures (Fig. 1). In this exercise, the Thalman &
26 Volkamer (2013) cross-sections at 203 and 293 K were used. When including only the room
27 temperature cross-section in the retrieval, the obtained O₄ is 3-5 % too large.

28 Our results agree with the very recent report by Spinei et al. (2014) who found a temperature
29 dependence of 9% for a variation of 44 K and no pressure dependence based on direct sun and
30 aircraft MAXDOAS measurements. The conclusion of their work is that no corrections need
31 to be made for effective temperatures near 275 K. Since the present method uses only the

1 horizontal path, the temperature along the path is nearly constant and the seasonal variability
2 in the subtropical FT is small. Air temperature at the level of Izaña ranges from 277 K in
3 January-February to 287 K in July-August. Consequently, no more than 2 % of error is
4 expected due to this effect.

5 Typical NO₂ SCD root mean square error of the fit for horizontal geometry is of 3×10^{14}
6 molec cm⁻². These errors represent 15–20 % of the typical differential SCD. A summary of
7 the analysis errors is shown in Table 1.

8

9 **3 The Izaña observatory and dataset**

10

11 Izaña (28.3°N, 16.5°W) is a well known GAW-NDACC station located at the top of the Izaña
12 mountain, one of the peaks of the great crater of the Teide volcano, at 2370 m a.s.l., in
13 Tenerife Island. The observatory and related meteorology has been extensively described in
14 previous publications (i.e. Rodriguez et al., 2009; Cuevas et al., 2013). It is representative of
15 the FT at night. During daytime it is frequently affected by anabatic winds resulting from
16 heating of the ground. This upslope breeze carries boundary layer air masses to the FT. The
17 intensity of the wind peaks near the local noon and can extend well into the afternoon. It can
18 be indirectly quantified using the measurements of water vapour on the station since air
19 masses from below carry high humidity to the height of the observatory. The measurements
20 of in situ NO₂ are also useful for this purpose, since the BL NO₂ concentrations in populated
21 areas near the coast are typically more than one order of magnitude larger than the
22 background FT.

23 For the present work only the horizontal spectra are analyzed. If the SZA was lower than 10°,
24 then the 70° elevation spectrum was used as reference to avoid spectral distortions due to too
25 short integration times. In all other cases the reference was the zenith spectrum of the same
26 cycle.

27 Data from three complete years (2011-2013) have been used after screening for (a) NO₂
28 RMSE: Fit error is limited to 2×10^{15} molec cm⁻² and a signal to noise ratio of 0.5, which is
29 approximately the detection limit of the instrument. (b) High SZA: Only data corresponding
30 to data below SZA 70° are used in the present analysis to limit the error in the path
31 calculations. (c) Aerosol loading: Measurements on days with Aerosol Optical Depth (AOD)

1 at 500 nm over 0.1, were rejected. (d) Length of the path: Individual measurements with paths
2 shorter than 30 km were also rejected (broken clouds or narrow dust layers might cause this
3 effect). (e) Unrealistic negative values appearing occasionally. Over 15.000 of data passed all
4 filters for the 3 years period (40% of all possible data).

5

6 **4 The Optimal Estimation Method**

7 The Optical Estimation Method (OEM) has been extensively used on last years to obtain NO₂
8 vertical profiles on moderate to high polluted environments. However, on free troposphere
9 background conditions, the concentrations are near the instrumental detection limit (10-100
10 pptv) and in these conditions the method provide unrealistic profiles. In this work we have
11 used it only to characterize the vertical distribution of the plume in a particular case study in
12 which a high NO₂ air mass arrived to the station. The mean AOD-500 nm on the studied day
13 was of only 0.02. **Under these conditions the impact of the aerosol loading in the retrieval is**
14 **very low. A test with and without aerosols yield mean differences of 1.46% in the retrieval for**
15 **heights between 1 and 5 km. Since uncertainties in the OEM method are larger than that**
16 **value,** aerosols have not been included in the analysis.

17 Given a set of measurements \mathbf{y} with the errors covariance \mathbf{S}_ϵ , the OEM (Rodgers, 2000)
18 provides the state vector \mathbf{x} that maximizes the probability that \mathbf{x} , containing the trace gas
19 vertical distribution, belongs to the interval $[\mathbf{x}, \mathbf{x}+d\mathbf{x}]$. Following OEM approach, the
20 maximum a posteriori solution $\hat{\mathbf{x}}$ is calculated as:

$$21 \hat{\mathbf{x}} = \mathbf{x}_a + \mathbf{S}_a \mathbf{K}^T (\mathbf{K} \mathbf{S}_a \mathbf{K}^T + \mathbf{S}_\epsilon)^{-1} (\mathbf{y} - \mathbf{K} \mathbf{x}_a) = \mathbf{x}_a + \mathbf{G}_y (\mathbf{y} - \mathbf{K} \mathbf{x}_a)$$

22 Where the weighting functions matrix \mathbf{K} express the sensitivity of the measurements to
23 variations in the trace gas profile (NO₂ in this case). In this work, \mathbf{K} is obtained with the
24 SPSSDISORT pseudo-spherical radiative transfer solver of the libRadtran software package
25 (Mayer and Kylling, 2005). The \mathbf{x}_a vector and \mathbf{S}_a matrix correspond to an a priori NO₂ profile
26 and its corresponding error covariance matrix, respectively.

27 The gain matrix \mathbf{G}_y , given by the following expression, quantifies the sensitivity of the
28 retrieval to the measurements:

$$G_y = S_a K^T (K S_a K^T + S_\epsilon)^{-1}$$

The averaging kernel matrix \mathbf{A} , is then obtained as follows:

$$A = G_y K$$

\mathbf{A} expresses the sensitivity of the retrieval to the true state, and it has an important role in the characterization of the retrieval. The retrieval at a given altitude is an average of the total profile weighted by the corresponding row of \mathbf{A} , also known as Averaging Kernel function (AK). In general, the AKs are functions with a single peak in the appropriate level, where the measurement provides additional information to add to the a priori profile. Trace of \mathbf{A} provides the independent pieces of information that can be extracted from the retrieval, usually known as degrees of freedom (DFS). **Typical values of the DFS in our retrievals are around 1.8.**

Another parameter **determining** the quality of the retrievals is the total error of the state vector elements. This parameter is the addition of three contributions: (1) the smoothing of the true profiles given by \mathbf{S}_a ; (2) The systematic errors of the measurements, provided by \mathbf{S}_ϵ ; and (3) systematic errors of the forward model mainly provided by the uncertainties in the parameters characterizing the atmosphere. **Average total error (considering the three mentioned contributions) for all the considered profiles and altitudes ranging from 1 to 5 kms is 9.1E-3 ppb.** The choose of the values corresponding to these three sources of error (\mathbf{S}_a , \mathbf{S}_ϵ and the atmosphere parameters) in our study will be described in the following paragraphs.

The NO_2 hourly profiles used as a priori profiles in our calculations were obtained using a photochemical box model (Denis et al., 2005) derived from the SLIMCAT 3-D chemical transport model (Chipperfield, 2006). Diagonal elements of \mathbf{S}_a are usually chosen to be a percentage of x_a . In this case, following the L-curve method described in (Schofield, 2003), they have been set to 100% of x_a , and its non-diagonal elements are calculated as follows (Barret et al., 2002; Friess et al., 2006):

$$S_{aij} = \sqrt{S_{a_{ii}} S_{a_{jj}} \exp(-\ln 2) \left(\frac{(z_i - z_j)}{\gamma} \right)^2}$$

Where z_i and z_j are the altitudes of the altitude grid levels i and j respectively, and γ is a half of the correlation length. The functions represented in the last equation are Gaussian

1 correlation functions which account for correlations between trace gas concentrations at
2 different altitudes. After several tests on the retrieval, γ value has been chosen to be 300 m,
3 correspondings to the value (between 0.1 and 1 km) that maximizes the DFS (trace of \mathbf{A}), for
4 the overall retrieval as well as for the altitudes closer to the station (2.3-2.6 km).

5 In this work, y represents the differential slant column densities (DSCD) of NO_2 measured
6 with the MAX-DOAS spectrometer, and \mathbf{S}_ϵ is set to a diagonal matrix which diagonal
7 elements correspond to the molecular errors of the measurements.

8 Concerning parameters characterizing atmosphere in our calculations, vertical profiles of O_3 ,
9 O_2 , CO_2 and H_2O have been obtained from the standard atmosphere for tropical latitudes
10 (Anderson, 1986). Radio-sounding data performed the same day of our calculations provided
11 the pressure, temperature and air density vertical profiles used in our retrieval. We have
12 considered layers of 100 m from 0 to 10 km, and with the same width of those corresponding
13 to the standard atmosphere for tropical latitudes (Anderson, 1986) for altitudes over 10 km. In
14 this work, AKs are near zero for altitudes lower than 0.5 km and higher than 5 km (see Fig.
15 2). The retrieved profiles have been obtained for altitudes up to 6 km.

16

17 **5 Model description and trajectory analysis**

18 CAM-Chem (Community Atmosphere Model with Chemistry) is a global 3D chemistry-
19 climate model fully integrated into the CESM framework (Community Earth System Model)
20 (Lamarque et al., 2012). In this work CAM-Chem has been configured using a horizontal grid
21 resolution of 1.91° latitude \times 2.5° longitude and 26 hybrid vertical levels from the surface to
22 approximately 38 km. All simulations have been performed in Specified dynamics (SD),
23 using offline meteorological fields to compute the atmospheric transport, considering the
24 same high frequency meteorological input from a previous CAM-Chem 15 years simulation.
25 This implies that the model is forced to evolve as if it were a Chemical Transport Model.

26 The model includes the tropospheric chemistry mechanism of MOZART-4 , implementing
27 also organic and inorganic halogen (chlorine, bromine and iodine) photochemistry
28 mechanism, taking into account natural and anthropogenic sources, heterogeneous recycling
29 and dry and wet deposition (Saiz-Lopez et al., 2012; Ordoñez et al., 2012; Fernandez et al.,
30 2014). Anthropogenic emissions due to fossil fuel and biofuel combustions come from the
31 POET (Precursors of Ozone and their effects in the troposphere) database for 2000 .

1 To investigate the air masses reaching the area of study, back trajectories were computed
2 with the HYSPLIT (Hybrid Single-Particle Lagrangian Integrated Trajectory) model,
3 developed by the NOAA's Air Resources Laboratory (ARL) (Draxler et al., 2009). The
4 ECMWF (European Centre for Medium Range Weather Forecasts) meteorological fields were
5 used with a spatial resolution of $0.25^{\circ} \times 0.25^{\circ}$, 22 vertical levels from the surface to 250 mb
6 and a time resolution of 6 h. Three-dimensional kinematic back trajectories were calculated. A
7 daily back-trajectory at 12:00 UTC, with a 168 h pathway (7 days) and at 2370 m a.s.l. was
8 computed. Following the HYSPLIT model tools back trajectories have been grouped in
9 clusters (Stunder, 1996), arriving at the Izaña observatory.

10

11 **6 Results and discussion**

12 **6.1 MAXDOAS vs. in situ**

13 Results of the NO_2 comparison can be classified according to three different meteorological
14 regimes. A period in 2013 has been selected to illustrate the differences in concentration
15 between the in situ local sampling and the MAXDOAS long-path average (Fig. 4, upper
16 panel). On days when the breeze is inhibited, the in situ data are representative of the FT, and
17 the agreement between instruments is very good (e.g. days 139-145). On days when anabatic
18 winds are present, NO_2 vmr increases are observed in the in situ measurements whereas
19 MAXDOAS signal remains at typical FT levels (e.g. days 130-137). Upslope winds cause an
20 air mass mixture with that associated by the FT synoptic wind. The upslope strength will
21 depend inversely on the intensity of the zonal synoptic winds. (Cuevas et al., 2013). In
22 general, the depth of the layer is not enough to contaminate the MAXDOAS path. This
23 situation is the one most commonly observed at Izaña. As expected, MAXDOAS provide a
24 much better representation of the FT background reactive gases. A third set of measurements
25 is shown when MAXDOAS data also suffer large increases (e.g. days 127-129). After
26 excluding thunderstorms with electric activity and wildfires in the area, it was found that this
27 situation always takes place in presence of southern winds. The only identified NO_2 large
28 source upwind is the 980 MW thermal power plant located 25 km south of Izaña, with a NO_2
29 emissions of $4.7 \times 10^6 \text{ kg year}^{-1}$. As previously reported (Persson and Grazzini, 2007), the
30 thermal local circulations are not captured by atmospheric global models even by the
31 ECMWF $0.25^{\circ} \times 0.25^{\circ}$ used in this study which predicted trajectories above 2000 m all the

1 way (Fig. 3, lower right). This orographically-forced lifting mechanism has been found to be
2 an efficient and fast way for irreversible transport of surface air to the FT. Pollutants and
3 minor gases of oceanic origin (i.e. IO, BrO) move upslope crossing the MBL top in less than
4 1 h, and then are subsequently mixed with FT air. The quantification of the amount of air
5 mass transported from the lower layers of the MBL to the FT is out of the scope of this work,
6 but certainly data provide evidence for the existence of an efficient and fast mechanism to
7 supply halogens and other marine trace gases to the FT. Since southern wind conditions are
8 common during the summer months (50 % of the days) and the mountain rift has a NE-SW
9 orientation, and a length of about 30 km, the supply of marine trace gases to the FT might be
10 not negligible, at least on a local scale.

11 Surprisingly, the very high MAXDOAS vmr reach as much as a half of the levels observed by
12 the in situ sensor. This is related to the pointing direction of the DOAS spectrometer, since the
13 plume propagates northward, along the same direction of the spectrometer line of sight. The
14 path within the plume results in an enhancement of the absorption signal. Figure 4 shows the
15 NO₂ vmr vertical cross sections for the day 128/2013, obtained by using the OEM technique,
16 indicating that the enhancement takes place near the level of the station, with an upper limit
17 around 4 km. This confirms that once the air mass passes over the mountain obstacle it either
18 moves horizontally or descends again but remaining in the FT. Note that the instrument
19 scanning lowest angle is below the horizon (IEA = -1°), thus containing information about the
20 trace gas concentration below the station.

21 It is worth to mention that Southern winds are generally related to African air masses
22 containing Saharan dust and, as previously mentioned, those dusty days were filtered out from
23 the analysis. The only non-dusty south wind cases observed are from Atlantic air masses
24 which suffered an abrupt change in direction when approaching to Africa. Consequently the
25 impact of this effect on the overall dataset is small. Only five clear cases have been identified
26 within the 3-year record. Those cases have been removed for seasonal evolution studies.

27 Figure 4 (top panel) shows the NO₂ vmr seasonal evolution separated by year. The seasonal
28 behavior is similar in all three years, with the maximum in the summer months and the
29 minimum in winter time. Summer gaps result from the large number of Saharan dust
30 intrusions during these months. To explore a possible dependence of the retrieved
31 concentrations with the SZA, the data have been plotted in colors according the SZA (Fig. 5,
32 mid panel). The maxima in summer months are observed regardless the SZA excluding the

1 possibility of stratospheric contamination or any other SZA dependent artifact. The
2 magnitudes of the retrieved concentration are also independent of the RMSE (Fig. 5, lower
3 panel). Sporadic peaks over 100 pptv are observed with no increase in typical retrieval errors.
4 The scattering along the day is also large with standard deviations of 10-15 pptv.
5 Monthly means clearly show the rapid spring build-up and the autumn decay (Fig. 6). Mean
6 values range from 20 to 44 pptv throughout the year. A summer maximum has previously
7 been found in unpolluted continental China in the boundary layer as result of soil biogenic
8 NO emissions (Van der A et al., 2006, Qi et al., 2014). However, NO₂ in long paths over the
9 Atlantic FT cannot be explained in this way. The output of the CAM-Chem model for the
10 location and the level of the station show similar results. The agreement with observational
11 data is particularly good for the period November to February. The NO₂ summer build-up
12 takes place across the entire FT (not shown). The winter to summer ratio is largest in the
13 middle troposphere at 8 km height. The peak FT NO₂ values occurring in summer was
14 previously observed by Val-Martin et al (2008), who attributed the summer maxima in NO₂ to
15 North American biomass burning during this season. The model results show no seasonal
16 differences in the NO₂ chemical formation/loss channels. However, an increase in the overall
17 reactive nitrogen budget occurs in this unpolluted FT site, as summer proceeds. We have
18 explored two possibilities to explain the seasonality of our observations:

19 **6.1.1 Contamination by anabatic winds**

20 It has been previously shown that MAXDOAS-MGA technique minimizes the unwanted
21 effects of MBL on FT measurements, but in principle, the influence of a potential seasonal
22 cycle in the intensity of the upwelling wind cannot be entirely ruled out. Since anabatic winds
23 are driven locally by surface heating, the depth of the layer of influence is expected to be of
24 only a few hundreds of meters but there is not enough information to quantify the size of this
25 depth and thus the potential contribution of a possible path contamination from air masses
26 rich in NO₂ coming from below. Most of the works available in the literature refer to the BL,
27 generally with return flow back. However, cases of upwelling to the FT are reported as well.
28 As early as 1923, Wenger (1923) observed this situation at the slopes of the Teide mountain
29 in Tenerife to up of 1500 m a.s.l. but no data were available above that height. In situ data in
30 Fig. 1 show evidence of MBL nitrogen oxides transported by anabatic winds up to the level of
31 the station (2370 m a.s.l.). However, an intensification of the upslope breeze in summer with

1 respect to winter would result in a larger vertical extension of the upwelling layer, increasing
2 its relative contribution in the MAXDOAS path. Out of the few large pollution cases, the
3 concentrations measured are too low for the OEM technique to be applied. It is nevertheless
4 unlikely that the summer increase in upwelling can account for the twofold increase in the
5 background NO₂ vmr. For instance, for a layer of 200 m with a NO₂ load of as high as 600 ppt
6 would represent an increase in the column of some 5-10 % of the background concentration
7 for a clean day.

8 We have recalculated NO₂ monthly means only from the first morning data, namely data
9 between SZA 70° a.m. and 65° a.m. These SZA correspond to fractional days ranging from
10 0.42 in mid winter to 0.32 in summer. At this early time of day the anabatic wind is still under
11 the first stage of development and the intensity of the upwelling is of only a few percent of the
12 maximum value after noon. Results show that the seasonality in the SZA 65° to 70° data is
13 almost identical than that when considering data at all SZA (ratio >0.98). We therefore
14 conclude that the summer increase is not a result of the contamination by high NO₂ upwelled
15 MBL air masses.

16

17 **6.1.2 Changes in horizontal transport patterns along season**

18 Val-Martin et al. (2008) analysed NO₂ mountain data from Azores and reported larger
19 summer concentrations attributed to North American biomass burning. However, circulation
20 at the lower latitudes of Canary Island is quite different. Attempts to determine the global FT
21 distribution of NO₂, based on the cloud slicing technique, have recently been made with OMI
22 data (Choi et al, 2014), but the method does not provide results in summer over the Sahara
23 region due to lack of cloudiness.

24 HYSPLIT 7 days back trajectory cluster analysis shows that airmasses arriving to Izaña
25 during the reporting period are fundamentally of Atlantic origin, with a small portion arriving
26 from Africa during the summer period (Fig. 7), in agreement with the 22-year (1988-2009)
27 backward trajectory climatology reported by Cuevas et al. (2013). As previously mentioned,
28 only NO₂ observations under no-dust conditions are considered, therefore days with African
29 trajectories are not included in the analysis. Winter trajectories are longer than the summer
30 ones and 30% of them cross the United States. All trajectory clusters show a steady
31 descendent transport in the last 96 hours prior to the arrival to Izaña and are originated at an

1 altitude of 4000-5500 m a.s.l.

2 The cluster analysis tells us that the origin of the NO₂ seasonal variation has to be searched in
3 the Western Atlantic area at much higher altitude than the station. The CAM-Chem model
4 sampled at the 5.9 km level shows larger summer values over North America and the
5 subtropical Atlantic, than in winter months, both in the range of the observed values (Fig. 8).
6 The phase of the mid-troposphere seasonal wave is opposite of the BL one (Lamsal et al.,
7 2010) and is probably due to a combination of seasonality in convection and lightning. Venting
8 processes from the BL to the FT over US has been studied (i.e. Parrish et al., 2004; Hudman
9 2007) finding export of NO_y, mainly in form of HNO₃ and PAN to the mid troposphere.
10 Convection is driven by surface insolation and has a clear seasonal wave. The same is true for
11 lightning since thunderstorms mainly occur during the spring-summer months.

12 Tropospheric vertical profiles (Fig. 9) show how NO₂ vmr are decreasing in wintertime from
13 the MBL to the mid FT whereas in summer the concentration remains constant up to 6 km
14 and then increases. At the 5 km level, the model shows differences from 15 to 40 pptv from
15 winter to summer. These calculated values are in agreement with the 40-50 pptv background
16 NO₂ vmr estimated by Choi et al., (2014) for the summer months FT in an extended area
17 covering the Western Atlantic from subtropics to mid latitudes.

18 The build-up is basically due to enhanced NO₂ formation via the NO+O₃ reaction under
19 higher concentration of NO as result of NO_y reconversion of PAN and HNO₃ in the FT. Note
20 that the lifetime of NO_y is long enough for NO_x-rich air masses, originated in North America,
21 to reach the African coast.

22 In summary, the NO₂ seasonal variation obtained from MAXDOAS measurements can be
23 explained with the help of the back trajectory cluster analysis and a chemistry-climate model
24 and result from a mixed effect of long-range transport and free tropospheric subsidence. This
25 is basically the same conceptual model that explains the origin or relatively high ozone values
26 recorded at Izaña in summertime described by Cuevas et al. (2013). The origin of the high
27 summer NO₂ values at Izaña is related to the larger background NO₂ vmr found over North
28 America in the mid FT, confirming earlier findings from Schultz et al. (1998).

29

30 **7 Summary**

31 NO₂ volume mixing ratio at the level of the high mountain observatory of Izaña (2370 m

1 a.s.l.) has been obtained for 3 years of data using the MAXDOAS technique and the recently
2 reported Modified Geometrical Approximation (MGA). The method uses the absorption of
3 the O₂-O₂ collisional complex at 477 nm to obtain the horizontal path and is applicable in a
4 near-Rayleigh atmosphere. Only data from airmasses of aerosol optical depths below 0.1 were
5 considered, thus removing African airmasses loaded with Saharan dust. Results show that on
6 most of the observation days, data are representative of the free troposphere. Exceptions are
7 found when wind blows from the South. On these occasions, we find evidence that
8 orographically forced surface airmasses ascend upslope to the Izaña observatory providing a
9 channel for irreversible transport of surface origin species to the free troposphere and might
10 provide an explanation for the concentrations of halogens oxides found in this region.

11 The NO₂ seasonal evolution shows a well defined annual cycle in phase with solar radiation.
12 Mean mixing ratios ranges from 20 pptv in mid winter to 42 pptv in summer with a
13 significant day to day variability. By contrast, we find a small interannual variability during
14 the 3-year observation period. A number of possible causes to explain the observed
15 seasonality have been discussed including seasonal changes in transport and contamination
16 due to seasonality in the upslope winds (anabatic winds) but they individually could not
17 provide an explanation of the observations. CAM-Chem climate chemistry model reproduces
18 the monthly distribution with great accuracy. The results of the back trajectory cluster
19 together with the model analysis show that the seasonality in NO₂ vmr is related to a
20 combined effect of long-range transport and subsidence in the free troposphere. Dust-free
21 trajectories follow North America/North Atlantic pathways with airmasses coming from the
22 mid-free troposphere, between 4000 and 5500 m a.s.l. The model and previous satellite
23 estimations show a seasonality in NO_y and NO₂ in the mid free troposphere in phase with the
24 MAXDOAS observations at Izaña. Larger summer values are probably due to a combination
25 of seasonality in convection and lightning.

26

27 **Acknowledgements**

28 This work was funded by the Spanish National R+D Funding Agency through project
29 AMISOC (CGL2011-24891) and the EU FP7 NORS project (Grant Agreement 284421). The
30 authors gratefully acknowledge NOAA Air Resources Laboratory for the provision of the
31 HYSPLIT transport and dispersion model.

1 **References**

- 2 Anderson, G. P.: AFGL atmospheric constituent profiles (0-120 km), Hanscom AFB, MA :
3 Optical Physics Division, Air Force Geophysics Laboratory, AFGL-TR ; 86-0110. U.S. Air
4 Force Geophysics Laboratory. Optical Physics Division, 1986.
- 5 Baidar, S., Oetjen, H., Coburn, S., Dix, B., Ortega, I., Sinreich, R., and Volkamer, R.: The
6 CU Airborne MAX-DOAS instrument: vertical profiling of aerosol extinction and trace
7 gases, *Atmos. Meas. Tech.*, 6, 719–739, 2013.
- 8 Barret, B., De Maziere, M. D., and Demoulin, P.: Retrieval and characterization of ozone
9 profiles from solar infrared spectra at the Jung-fraujoch, *J. Geophys. Res.* 107(D24), 4788,
10 doi:10.1029/2001JD001298, 2002.
- 11 Bradshaw, J., Newell, R., Sandholm S., and Liu, S.: Observed distributions of nitrogen oxides
12 in the remote free troposphere from the NASA Global Tropospheric Experiment Programs,
13 *R. Geophysics*, 38, 1, 2000.
- 14 Bucsel, E. J., Perring, A. E., Cohen, R. C. Boersma, K. F., Celarier, E. A. Gleason, J. F.,
15 Wenig, M. O., Bertram, T. H., Wooldridge, P.J., Dirksen, R., and Veefkind, J. P.:
16 Comparison of tropospheric NO₂ from in situ aircraft measurements with near-real-time
17 and standard product data from OMI, *J. Geophys. Res.*, V 113, D16S31,
18 doi:10.1029/2007JD008838, 2008.
- 19 Carroll, M.A., Hastie, D.R., Ridley, B.A., Rodgers, M. O., Torres, A. L., Davis, D. D.,
20 Bradshaw, J. D. Sandholm, S. T., Schiff, H.I., Karecki, D. R., Harris, G. W. Mackay, G. I.,
21 Gregory, G. L., Condin, E. P., Trainer, M., Hübler, G., Montzka, D. D., Madronic, S., H.,
22 Albritton, D. L., Singh, H. B., Beck, S. M., Shipham, M.C. and Bachmeier, A. S. Aircraft
23 Measurements of NO_x over the Eastern Pacific and Continental United States and
24 Implications for Ozone Production, *J. Geophys. Res.* V95, D7, pp 10.205-10.233, 1990.
- 25 Chipperfield, M. P.: New version of the TOMCAT/SLIMCAT off-line chemical transport
26 model: Intercomparison of stratospheric tracer experiments, *Q. J. R. Meteorol. Soc.*, 132,
27 1179–1203, doi:10.1256/qj.05.51, 2006.
- 28 Choi, S., Joiner, J., Choi, Y., Duncan, B. N., Vasilkov, A., Krotkov, N., and Bucsel, E.: First
29 estimates of global free tropospheric NO₂ abundances derived using a cloud slicing
30 technique applied to satellite observations from the Aura Ozone Monitoring Instrument

1 (OMI), *Atmos. Chem. Phys.*, 14, 10565–10588, doi:10.5194/acp-14-10565-2014, 2014.

2 Clémer, K., Van Roozendaal, M., Fayt, C., Hendrick, F., Hermans, C., Pinardi, G., Spurr, R.,
3 Wang, P., and De Mazière, M., Multiple wavelength retrieval of tropospheric aerosol
4 optical properties from MAXDOAS Measurements in Beijing, *Atmos. Meas. Tech.*, 3,
5 863–878, doi:10.5194/amt-3-863-2010, 2010.

6 Cuevas, E., González, Y., Rodríguez, S., Guerra, J. C., Gómez-Peláez, A. J., Alonso-Pérez,
7 S., Bustos, J., and Milford, C., Assessment of atmospheric processes driving ozone
8 variations in the subtropical North Atlantic free troposphere, *Atmos. Chem. Phys.*, 13,
9 1973-1998, doi:10.5194/acp-13-1973-2013, 2013.

10 Cuevas, C., Notario, A., Adame, J.A., Hilboll, A., Richter, A., Burrows, J. P. and A. Saiz-
11 Lopez, Evolution of NO₂ levels in Spain from 1996 to 2012, *Scientific Reports*, 4, 5887;
12 DOI:10.1038/srep05887, 2014.

13 Denis, L., Roscoe, H. K., Chipperfield, M. P., Van Roozendaal, M., and Goutail, F.: A new
14 software suite for NO₂ vertical profile retrieval from ground-based zenith-sky
15 spectrometers, *J. Quant. Spectrosc. Rad. Transf.*, 92, 321–333,
16 doi:10.1016/j.jqsrt.2004.07.030, 2005.

17 Draxler, R.R., Stunder, B., Rolph, G., Taylor, A. 2009. HYSPLIT_4 User's Guide, via NOAA
18 ARL website. NOAA Air Resources Laboratory, Silver Spring, MD, December 1997 (last
19 access: May 19, 2015), revised January 2009.
20 http://www.arl.noaa.gov/documents/reports/hysplit_user_guide.pdf

21 Emmons, L. K., Walters, S., Hess, P. G., Lamarque, J.-F., Pfister, G. G., Fillmore, D.,
22 Granier, C., Guenther, A., Kinnison, D., Laepple, T., Orlando, J., Tie, X., Tyndall, G.,
23 Wiedinmyer, C., Baughcum, S. L. and Kloster, S.: Description and evaluation of the Model
24 for Ozone and Related chemical Tracers, version 4 (MOZART-4), *Geosci. Model Dev.*,
25 3(1), 43–67, doi:10.5194/gmd-3-43-2010, 2010.

26 Fernandez, R. P., Salawitch, R. J., Kinnison, D. E., Lamarque, J.-F. and Saiz-Lopez, A.:
27 Bromine partitioning in the tropical tropopause layer: implications for stratospheric
28 injection, *Atmos. Chem. Phys.*, 14, 13391-13410, doi:10.5194/acp-14-13391-2014, 2014.

29 Flynn, C. M., Pickering, K. E., Crawford, J. H., Lamsal, L. N., Krotkov, N. A., Herman, J.,
30 Weinheimer, A., Chen, G., Liu, X., Szykman, J., Tsay, S. C., Laughner, C. P., Hains, J.,

1 Lee, P., Dickerson, R. R., Stehr, J. W., and Brent, L.: The relationship between column-
2 density and 20 surface mixing ratio: statistical analysis. *Atmos. Environ.* 92, 429-441,
3 2014.

4 Friess, U., Monks, P. S., Remedios, J. J., Rozanov, A., Sinreich, R., Wagner, T., and Platt, U.:
5 MAX-DOAS O₄ measurements: A new technique to derive information on atmospheric
6 aerosols: 2. Modeling studies, *J. Geophys. Res.*, 111, D14203, doi:10.1029/2005JD006618,
7 2006.

8 Gómez, L., Navarro-Comas, M., Puente-dura, O., Gonzalez, Y., Cuevas, E. and Gil-Ojeda, M.:
9 Long-path averaged mixing ratios of O₃ and NO₂ in the free troposphere from mountain
10 MAX-DOAS *Atmos. Meas. Tech.*, 7, 1-12, 2014.

11 Granier, C., Guenther, A., Lamarque, J. F., Mieville, A., Muller, J., Olivier, J., Orlando, J.,
12 Peters, J., Petron, G., Tyndall, G., and Wallens, S.: POET, a database of surface emissions
13 of ozone precursors, available at at: <http://www.aero.jussieu.fr/projet/ACCENT/POET.php>
14 (last access: May 19, 2015), 2005.

15 Heland, J., Schlanger, H., Richter A., and Burrows, J.P.: First comparison of tropospheric
16 NO₂ column densities retrieved from GOME measurements and in situ aircraft profile
17 measurements, *Geophys. Res. Lett.*, V29, N20, 1983, doi:10.1029/2002GL015528, 2002.

18 Hermans C., O₄ absorption cross-sections at 298K (335.59-666.63 nm), available at:
19 <http://spectrolab.aeronomie.be/index.htm> (last access: May 19, 2015), 2011.

20 Hilboll, A., Richter A., and Burrows, J. P.: Long-Term changes of tropospheric NO₂ over
21 megacities derived from multiple satellite instruments, *Atmos. Chem. Phys.*, 13, 4145–
22 4169, 2013.

23 Hudman, R. C., Jacob, D. J., Turquety, S., Leibensperger, E. M., Murray, L. T., Wu, S.,
24 Gilliland, A. B., Avery, M., Bertram, T. H., Brune, W., Cohen, R. C., Dibb, J. E., Flocke,
25 F. M., Fried, A., Holloway, J, Neuman, J. A., Orville, R., Perring, A., Ren, X., Sachse, G.
26 W., Singh, H. B., Swanson A., and Wooldridge, P. J.: Surface and lightning sources of
27 nitrogen oxides over the United States: Magnitudes, chemical evolution, and outflow, *J.*
28 *Geophys. Res.*, 112, D12S05, doi:10.1029/2006JD007912, 2007.

29 Irie, H., Sudo, K., Akimoto, H., Richter, A. Burrows, J. P., Wagner, T., Wenig, M., Beirle, S.
30 Kondo, Y., Sinyakov V. P. and Goutail, F.: Evaluation of long-term tropospheric NO₂ data

1 obtained by GOME over East Asia in 1996-2002, *Geophys. Res. Lett.*, V32, L11810,
2 doi:10.1029/2005GL022770, 2005.

3 Jacob, D.J., Crawford, J. H., Kleb, M- M., Connors, V. S., Bendura, R. J., Raper, J. L.,
4 Sachse, G. W., Gille, J. G., Emmons, L., and Heald, C. L.: Transport and Chemical
5 Evolution over the Pacific (TRACE-P) aircraft mission: Design, execution, and first
6 results, *J. Geophys. Res.*, V 108, NO. D20, 9000, doi:10.1029/2002JD003276, 2003.

7 Kleissl, J. K., Honrath, R. E., Dziobak, M. P., Tanner, D., Val Martín, M., Owen, R. C. and
8 Helmig, C.: The occurrence of upslope flows at the Pico mountain top observatory: A case
9 study of orographic flows on a small, volcanic island, *J. Geophys. Res.*, 112, D10S35,
10 doi:10.1029/2006JD007565, 2007.

11 Lamarque, J.-F., Emmons, L. K., Hess, P. G., Kinnison, D. E., Tilmes, S., Vitt, F., Heald, C.
12 L., Holland, E. A., Lauritzen, P. H., Neu, J., Orlando, J. J., Rasch, P. J. and Tyndall, G. K.:
13 CAM-chem: description and evaluation of interactive atmospheric chemistry in the
14 Community Earth System Model, *Geosci. Model Dev.*, 5(2), 369–411, doi:10.5194/gmd-5-
15 369-2012, 2012.

16 Lamsal R. N., Martin, R. V., van Donkelaar, A., Celarier, E. A., Bucsela, E. J., Boersma, K.
17 F., Dirksen, R., Luo, C. and Wang, Y.: Indirect validation of tropospheric nitrogen dioxide
18 retrieved from the OMI satellite instrument: Insight into the seasonal variation of nitrogen
19 oxides at northern midlatitudes. *J. of Geophys. Res.*, V. 115, D05302,
20 doi:10.1029/2009JD013351, 2010.

21 Mayer, B. and Kylling, A.: Technical note: The LibRadtran software package for radiative
22 transfer calculations – description and examples of use, *Atmos. Chem. Phys.*, 5, 1855–
23 1877, doi:10.5194/acp-5-1855-2005, 2005.

24 Ordóñez, C., Lamarque, J.-F., Tilmes, S., Kinnison, D. E., Atlas, E. L., Blake, D. R., Sousa
25 Santos, G., Brasseur, G. and Saiz-Lopez, A.: Bromine and iodine chemistry in a global
26 chemistry-climate model: description and evaluation of very short-lived oceanic sources,
27 *Atmos. Chem. Phys.*, 12(3), 1423–1447, doi:10.5194/acp-12-1423-2012, 2012.

28 Parrish D. D., Ryerson, T. B., Holloway, J. S., Neuman, J. A., Roberts, J. M., Williams, J.,
29 Stroud, C. A., Frost, G. J., Trainer, M., Hübler, G., Fehsenfeld, F. C., Flocke F., and
30 Weinheimer, A. J.: Fraction and composition of NO_y transported in air masses lofted from
31 the North American continental boundary layer, *J. Geophys. Res.*, V109, D09302,

- 1 DOI: 10.1029/2003JD004226, 2004.
- 2 Parrish D. D., Ryerson, T. B., Holloway, J. S., Neuman, J. A., Roberts, J. M., Williams, J.,
3 Stroud, C. A., Frost, G. J., Trainer, M., Hübler, G., Fehsenfeld, F. C., Flocke F., and
4 Weinheimer, A. J.: Fraction and composition of NO_y transported in air masses lofted from
5 the North American continental boundary layer, *J. Geophys. Res.*
6 DOI: 10.1029/2003JD004226, 2004.
- 7 Persson, A. and Grazzini, F., User Guide to ECMWF forecast products, *Meteorological*
8 *Bulletin M3.2*, Edited by ECMWF. Available at:
9 http://www.uio.no/studier/emner/matnat/geofag/GEF4220/v09/undervisningsmateriale/Persson_user_guide.pdf (last access May 19, 2015), Updated 2007.
- 10
- 11 Puentedura, O., Gil, M., Saiz-Lopez, A., Hay, T., Navarro-Comas, M., Gomez-Pelaez, A.,
12 Cuevas, E., Iglesias J., and Gomez, L.: Iodine monoxide in the North subtropical free
13 troposphere, *Atmos. Chem. Phys.*, 12, 4909–4921, doi:10.5194/acp-12-4909-2012, 2012.
- 14 Qi, Y.: Spatio-Temporal distributions of tropospheric NO₂ over Oases in Taklimakan Desert,
15 China, *Chin. Geogra. Sci.*, 1-8, doi:10.1007/s11769-014-0696-z, 2014.
- 16 Reidmiller D.R., Jaffee, D. A., Fischer E. V., and Finley, B.: Nitrogen oxides in the boundary
17 layer and free troposphere at the Mt. Bachelor Observatory, *Atmos. Chem Phys.*, 10, 6043-
18 6062, 2010.
- 19 Richter, A., Burrows, J. P., Nüs, H., Granier C., and Niemeier, U.: Increase in tropospheric
20 nitrogen dioxide over China observed from space, *Nature* 437, 129-132,
21 doi:10.1038/nature04092, 2005.
- 22 Ridley, B. A., Carroll, M. A., Gregory, G. L., and Sachse, G. W.: NO and NO₂ in the
23 troposphere: Technique and measurements in regions of a folded tropopause J., *Geophys.*
24 *Res.*, 93, 15,813-15,830, 1988.
- 25 Rodgers, C. D.: *Inverse Methods for Atmospheric Sounding: Theory and Practice*, vol. 2 of
26 *Atmospheric, Oceanic and Planetary Physics*, World Scientific, Hackensack, NJ,
27 doi:10.1142/9789812813718_fmatter, 2000.
- 28 Rodriguez, S., Y. Gonzalez, E. Cuevas, R. Ramos, P. M. Romero, J. Abreu-Afonso and A.
29 Redondas, Atmospheric nanoparticle observations in the low free troposphere during
30 upward orographic flows at Izana Mountain Observatory *Atmos. Chem. Phys.*, 9, 6319–

- 1 6335, 2009.
- 2 Saiz-Lopez, A., Lamarque, J.-F., Kinnison, D. E., Tilmes, S., Ordóñez, C., Orlando, J. J.,
3 Conley, A. J., Plane, J. M. C., Mahajan, A. S., Sousa Santos, G., Atlas, E. L., Blake, D. R.,
4 Sander, S. P., Schauffler, S., Thompson, A. M. and Brasseur, G.: Estimating the climate
5 significance of halogen-driven ozone loss in the tropical marine troposphere, *Atmos.*
6 *Chem. Phys.*, 12(9), 3939–3949, doi:10.5194/acp-12-3939-2012, 2012.
- 7 Chipperfield, M. P.: New version of the TOMCAT/SLIMCAT off-line chemical transport
8 model: Intercomparison of stratospheric tracer experiments, *Q. J. R. Meteorol. Soc.*, 132,
9 1179–1203, doi:10.1256/qj.05.51, 2006.
- 10 Schultz, M., Schmitt, R., Thomas, K., Volz-Thomas, A., Photochemical box modeling of
11 long-range transport from North America to Tenerife during the North Atlantic Regional
12 Experiment (NARE) 1993, *J. Geophys. Res.* 103, D11, 13477–13488, DOI:
13 10.1029/97JD01481, 1998.
- 14 Spinei, E., Cede, A., Herman, J., Mount, G. H., Eloranta, E., Morley, B., Baidar, S., Dix, B.,
15 Ortega, I., Koenig, T. and Volkamer, R.: Direct sun and airborne MAX-DOAS
16 measurements of the collision induced oxygen complex, O₂O₂ absorption with significant
17 pressure and temperature differences, *Atmos. Meas. Tech. Discuss.*, 7, 10015-10057, 2014.
- 18 Stunder, B. An assessment of the Quality of Forecast Trajectories. *Journal of Applied*
19 *Meteorology* 35, 1319-1331, 1996.
- 20 Thalman, R., and Volkamer, R. Temperature dependent absorption cross-sections of O₂-O₂
21 collision pairs between 340 and 630 nm and at atmospherically relevant pressure, *Phys*
22 *Chem Chem Phys.*, 15, doi: 10.1039/c3cp50968k, 2013.
- 23 Vandaele, A. C., Hermans, C., Simon, P. C., Carleer, M., Colins, R., Fally, S., Mérienne, M.
24 F., Jenouvrier, A., and Coquart, B.: Measurements of the NO₂ Absorption Cross-Sections
25 from 42000 cm⁻¹ to 10000 cm⁻¹ (238–1000 nm) at 220 K and 294 K, *J. Quant. Spectrosc.*
26 *Ra.*, 59, 171–184, doi:10.1016/S0022-4073(97)00168-4, 1998.
- 27 Val-Martin, M., Honrath, R. E., Owen, R. C., and Li, Q. B.: Seasonal variation of nitrogen
28 oxides in the central North Atlantic lower free troposphere *J. Geophys. Res.*, V113,
29 D17307, doi:10.1029/2007JD009688, 2008.
- 30 Van der A., R. J., Peters, D. H. M. U., Eskes, H., Boersma, K. F., Van Roozendael, M., De

- 1 Smedt, I., and Kelder, H. M.: Detection of the trend and seasonal variation in tropospheric
2 NO₂ over China, *J. of Geophys. Res.*, V111, D12317, doi:10.1029/2005JD006594, 2006.
- 3 Wagner, T., Dix, B., Friedeburg, C.V., Friess, U., Sinreich, R., and Platt, U.: MAX-DOAS O4
4 measurements: A new technique to derive information on atmospheric aerosols –
5 Principles and information content, *J. Geophys. Res.*, 109, D22205, doi:10-
6 1029/2004JD0044904, 2004.
- 7 Wagner, T., von Friedeburg, C., Wening, M., Otten, C., and Platt, U.: UV-Visible
8 observations of atmospheric O4 absorptions using direct moonlight and zenith-scattered
9 sunlight for clear sky and cloudy sky conditions, *J. Geophys. Res.*, 107, 4424,
10 doi:10.1029/2001JD001026, 2002.
- 11 Wenger, R. Zur Theorie der Berg- und Talwinde', *Meteorol. Zeits.* 7, 193–204, 1923.
- 12 Wittrock, F., Oetjen, H., Richter, A., Fietkau, S., Medeke, T., Rozanov, A., and Burrows, J.
13 P.: MAX-DOAS measurements of atmospheric trace gases in Ny-Alesund – Radiative
14 transfer studies and their application, *Atmos. Chem. Phys.*, 4, 955–966, doi:10.5194/acp-
15 4-955-2004, 2004.
- 16 Ziemke, J. R., Chandra, S., and Bhartia, P. K.: “Cloud slicing”: a new technique to derive
17 upper tropospheric ozone from satellite measurements, *J. Geophys. Res.*, 106, 9853–9867,
18 2001.
- 19 Zien, A.W., Reichter, A., Hillboll, A., Blechschmidt A.-M., and Burrows, J. P.: Systematic
20 analysis of tropospheric NO₂ long-range transport events detected in GOME-2 satellite
21 data, *Atmos. Chem Phys.*, 14, 7367-7396, doi:10.5194/acp-14-7367-2014, 2014.

1
2
3
4
5
6
7
8
9
10
11
12

| Table 1. Method uncertainty | |
|--|------------------------------|
| Uncertainty in NO ₂ due to fit | 15-20% |
| Uncertainty in path due to the O ₄ fit | < 1% |
| Uncertainty of the method (related to unknown vertical distribution of NO ₂ and actual effective path) | 2.5-9% (for sza: 50° to 70°) |
| Error in horizontal path due to O ₄ cross-sections temperature dependence | 2% |
| OVERALL UNCERTAINTY | 20-32% |

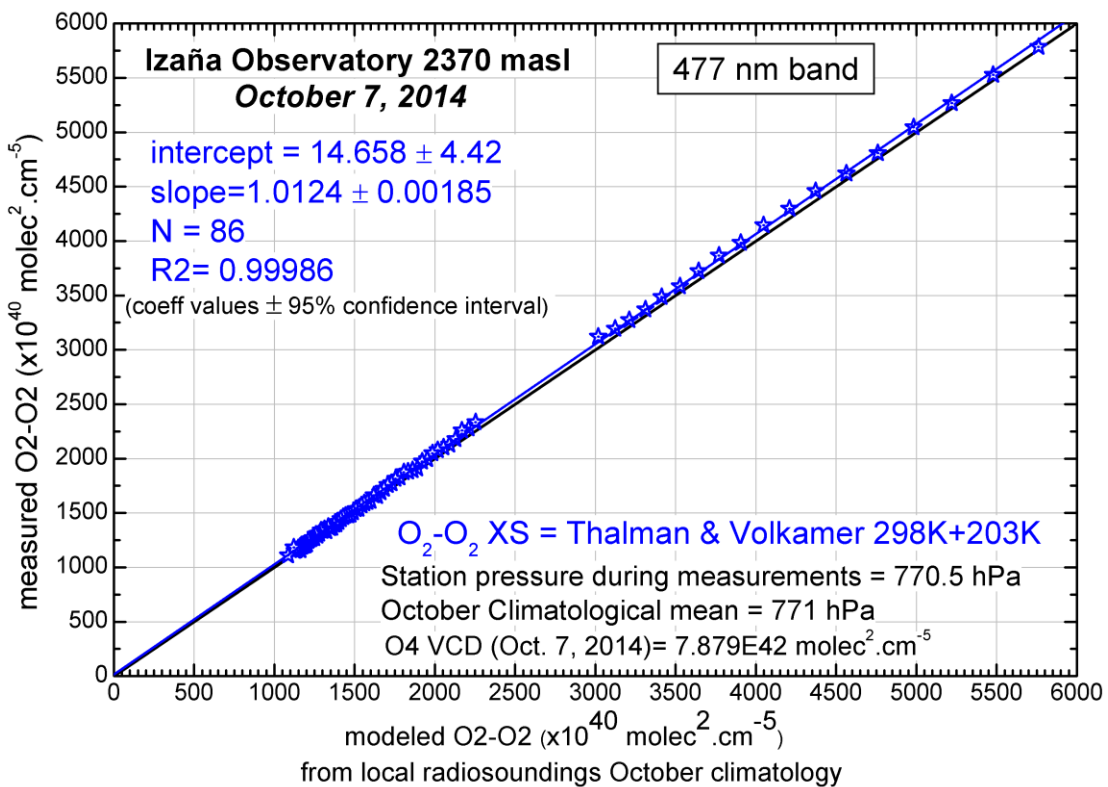
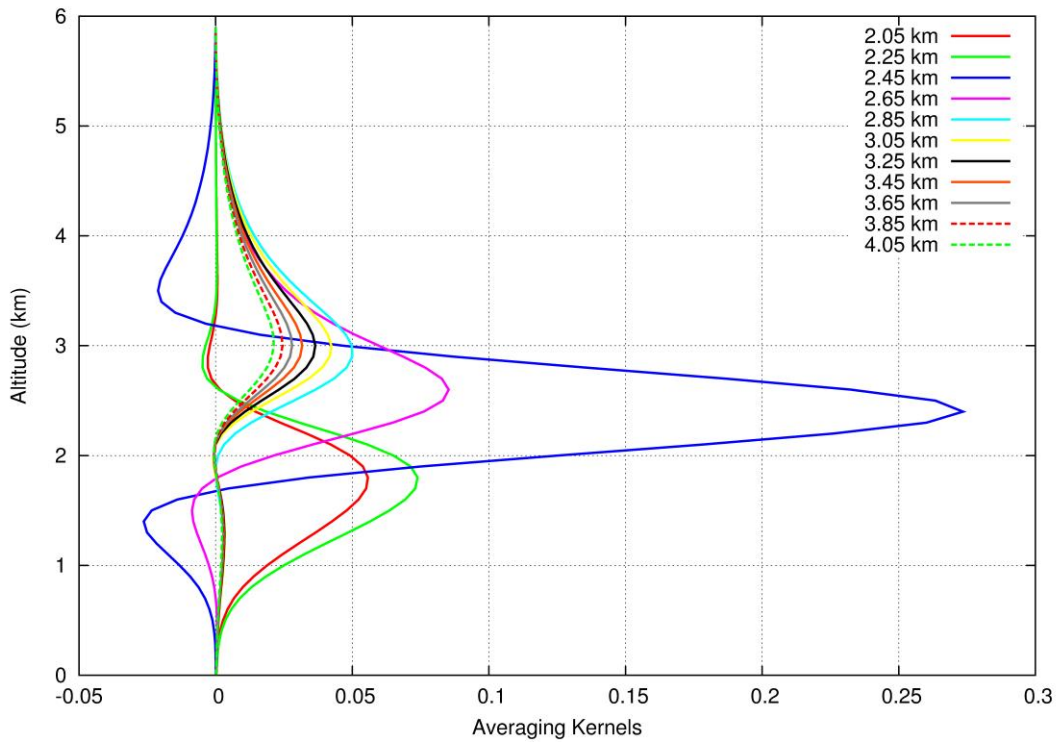


Figure 1. Measured O₄ SCD versus modeled O₄ for a pure Rayleigh atmosphere at the 477 nm band by using cross-sections at 203K and 293K temperatures (see text for details)

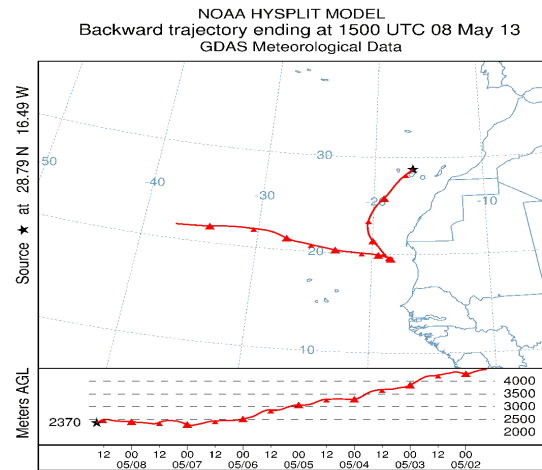
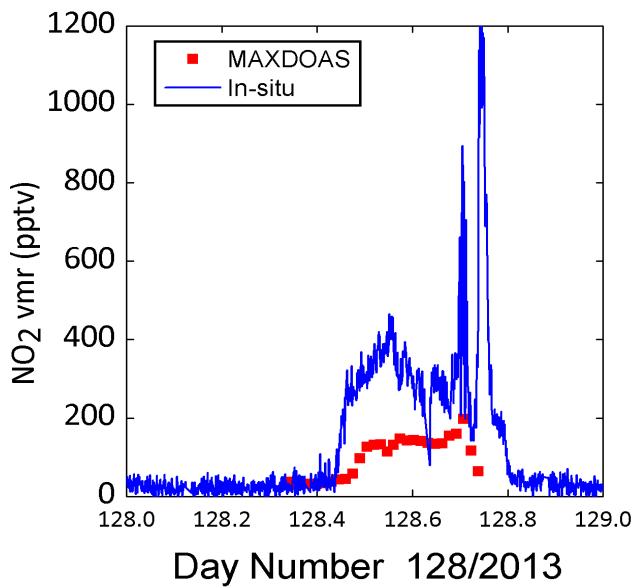
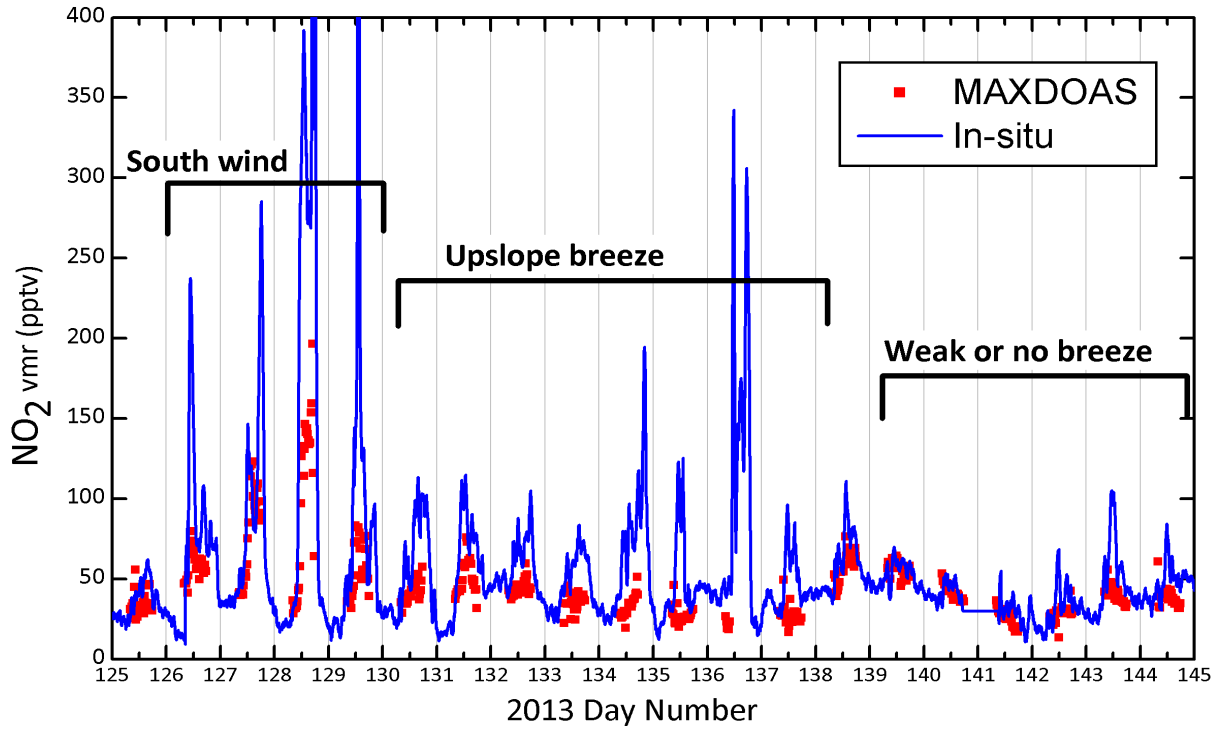


1

2

3 Figure 2. **Laura**

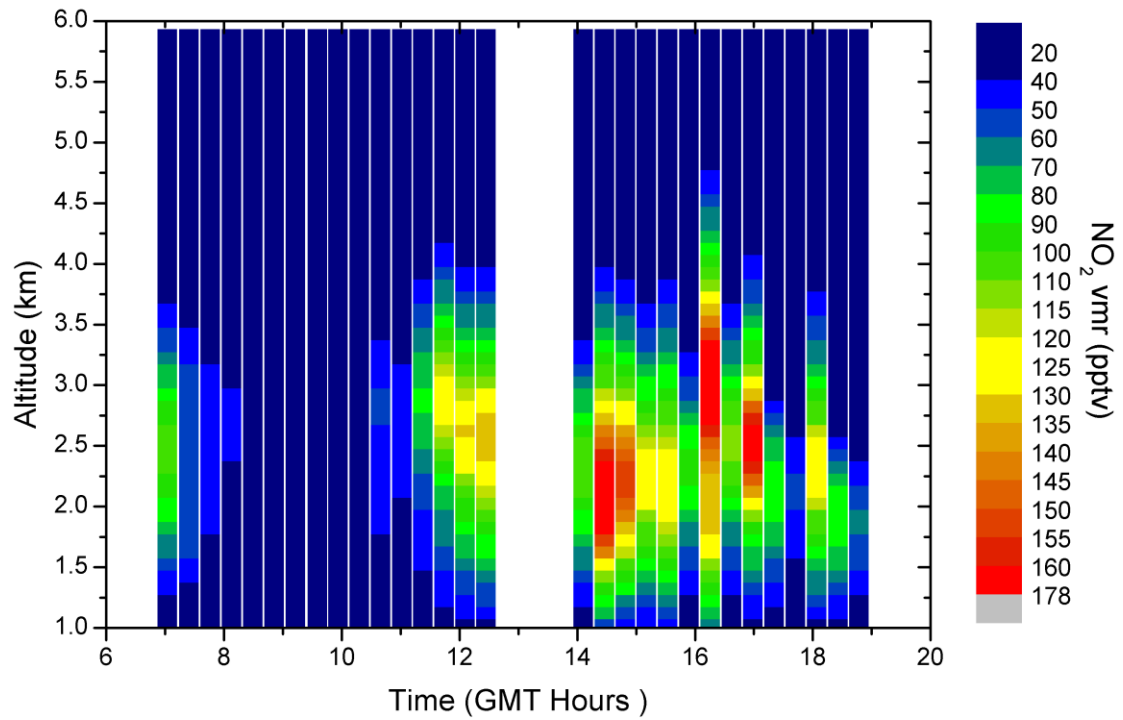
1



2

3 Figure 3. Izaña MAXDOAS versus minutal in-situ NO₂ volume mixing ratio for a period of
4 time representative of 3 different wind situation. *In-situ* data are smoothed by 50-minutes
5 running mean. (Top panel). Expanded plot for day May 8, 2013 (day number 128).
6 Backtrajectory ending at Izaña at 15h of the same day.

7

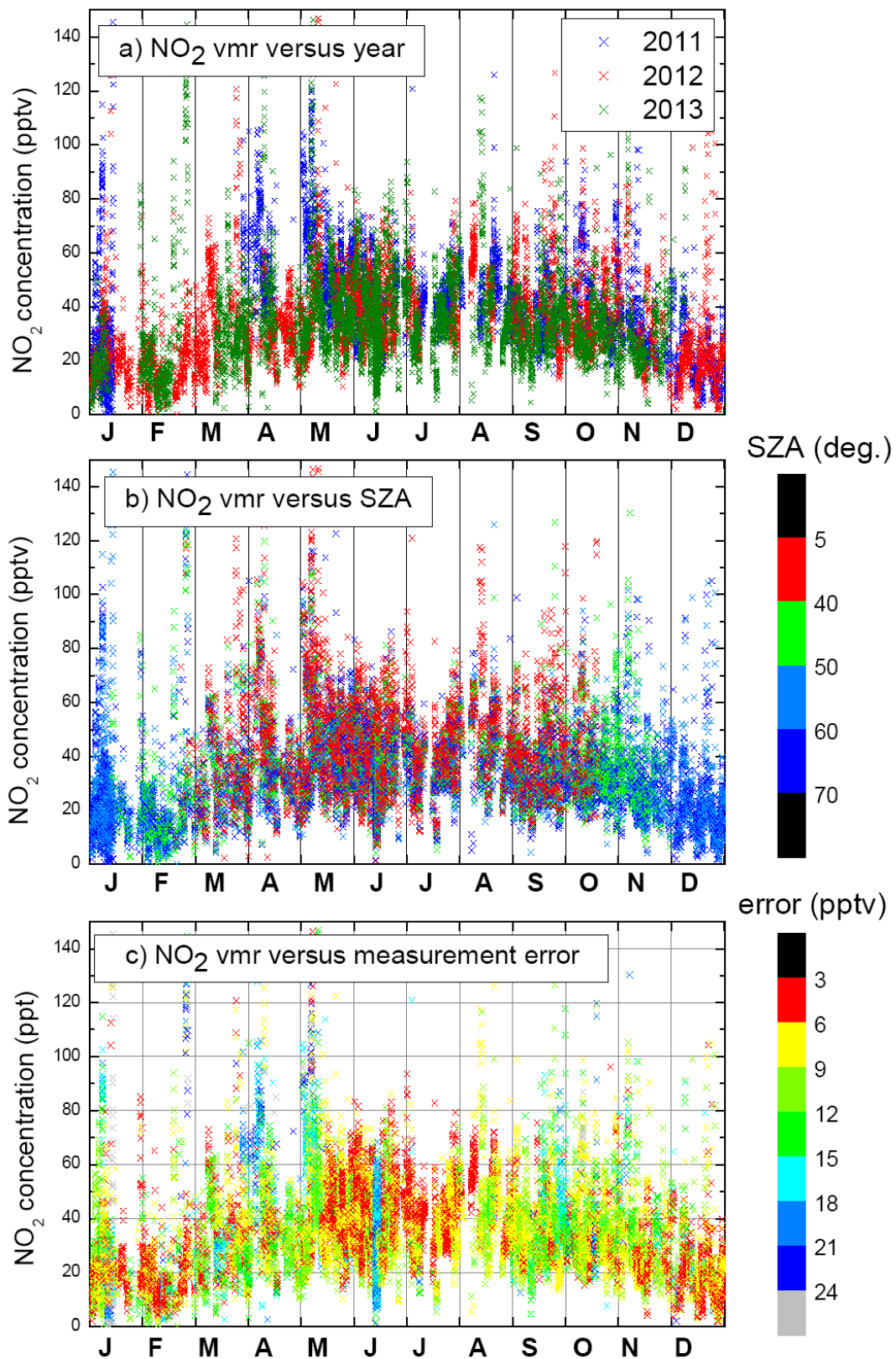


1

2 Figure 4. Unsmoothed vertical profiles of NO₂ vmr (in ppbv) for day 128/2013 obtained by
 3 OEM technique. Each vertical column represents an individual scanning cycle. (For details
 4 [see text](#))

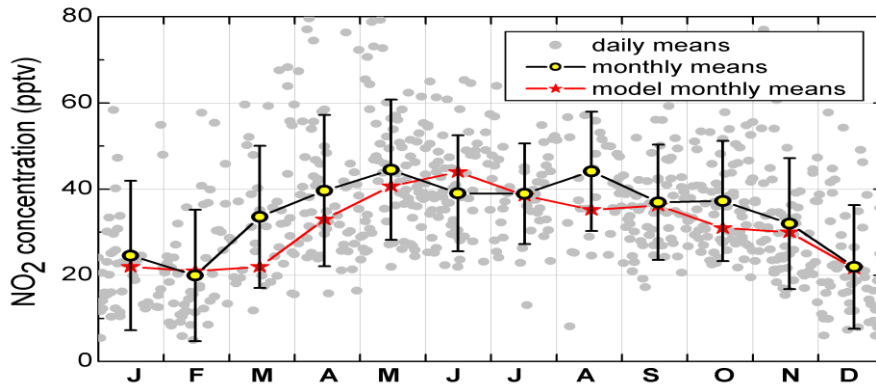
5

6



1
 2 Figure 5. Seasonal evolution of the individual data NO₂ vmr separated by years (Upper
 3 panel). Separated by Solar Zenith Angles (Mid panel) and separated by RMSE (Lower panel).

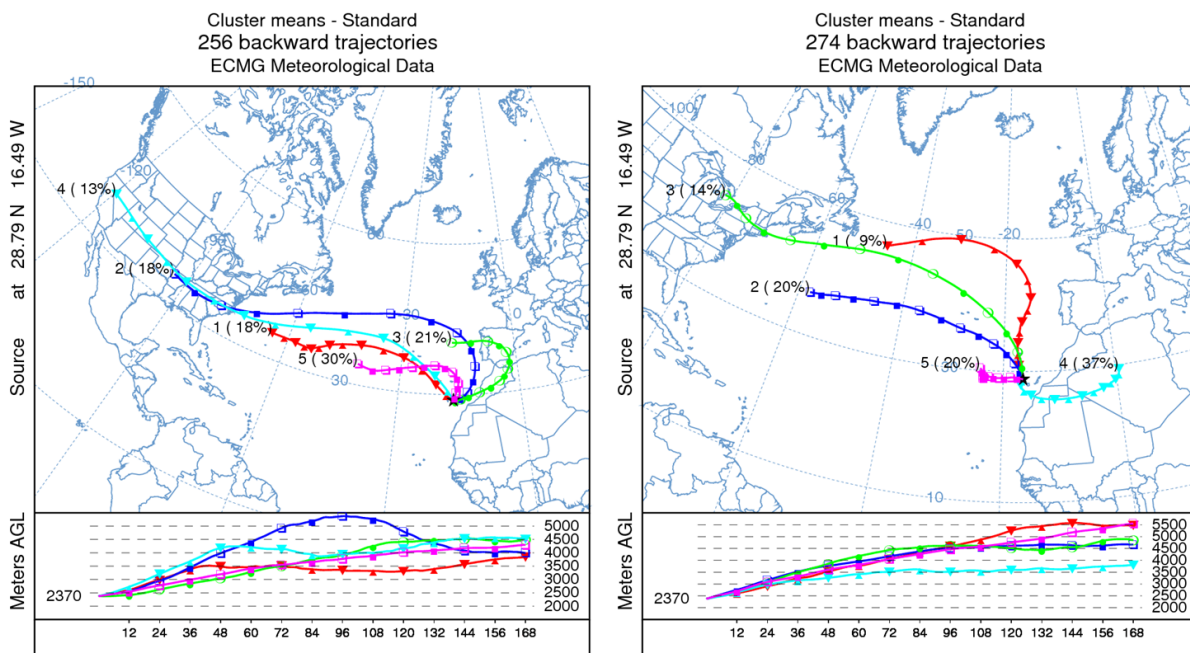
1



2

3 Figure 6. NO₂ concentration monthly means at the level of Izaña Observatory with their
 4 respective standard deviations (open circles and black lines). CAM-Chem model results for
 5 the same level are shown for comparison (Red stars and lines). Individual solid grey circles
 6 are the 3-years diurnal mean

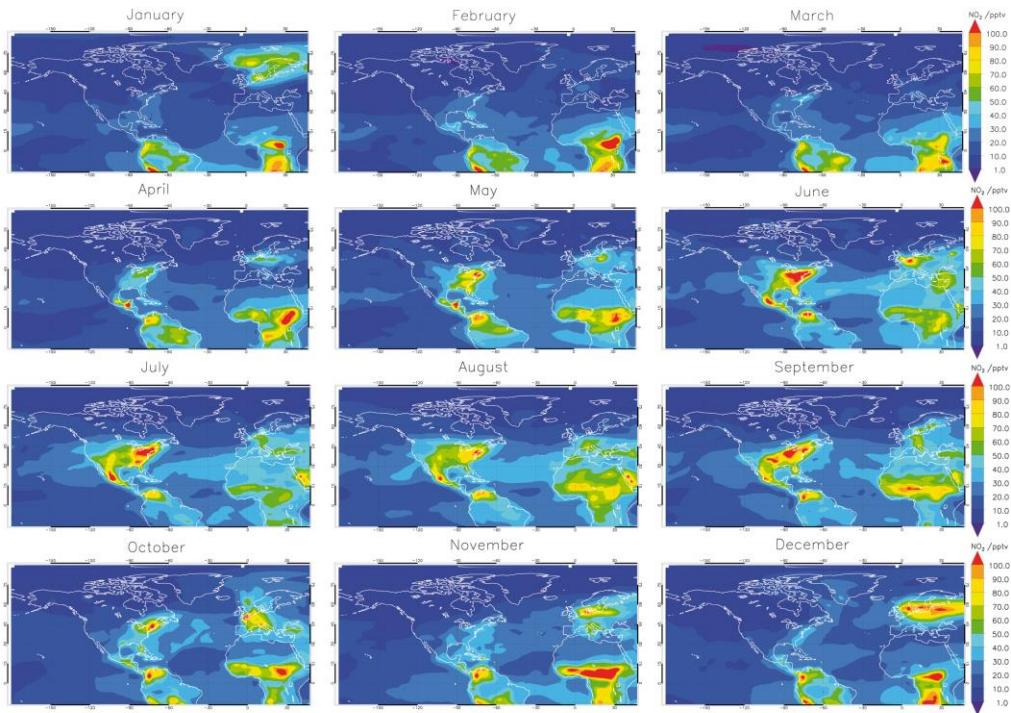
7



8

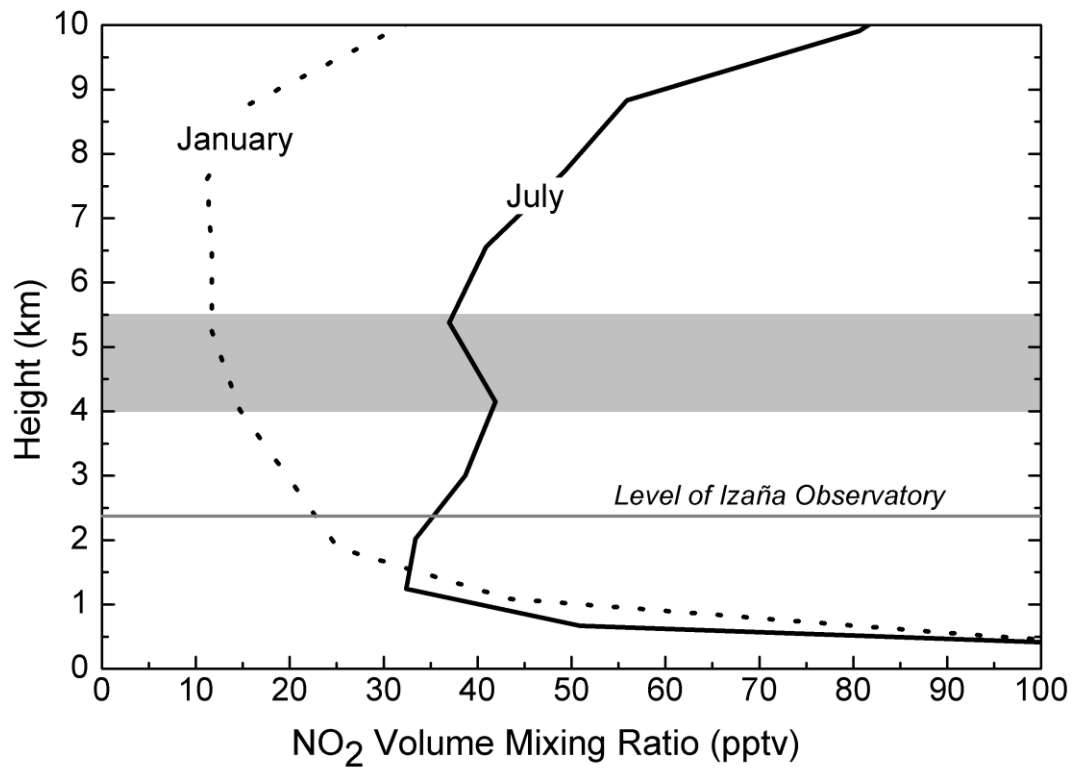
9 Figure 7. 1-week HYSPLIT back trajectories clusters arriving to Izaña Observatory for the
 10 left panel: winter months (DJF), right panel: summer months (JJA) and years 2011-2013

11



1

2 Figure 8. Global distributions of monthly mean NO₂ vmr for the level 5.9 km obtained from
 3 the Cam-CHEM chemistry climate model-model.



1

2 Figure 9. NO₂ vmr monthly means vertical profiles from Cam-CHEM model.

3 Gray band represents the height range where airmasses are originated (see text).